

# Supporting Information for "Constraining an ocean model under Getz Ice Shelf, Antarctica, using a gravity-derived bathymetry"

Romain Millan<sup>1,2</sup>, Pierre St-Laurent<sup>3,4</sup>, Eric Rignot<sup>2,5,6</sup>, Mathieu Morlighem<sup>2</sup>,  
J. Mouginot<sup>1,2</sup>, B. Scheuchl<sup>2</sup>

<sup>1</sup>Univ. Grenoble Alpes, CNRS, IRD, Grenoble INP, IGE, 38000 Grenoble, France

<sup>2</sup>University of California Irvine, Dept. Earth System Science, Irvine, CA 92697

<sup>3</sup>Center for Coastal Physical Oceanography, Old Dominion University, Norfolk, Virginia, USA

<sup>4</sup>Virginia Institute of Marine Science, William & Mary, Gloucester Pt, Virginia, USA

<sup>5</sup>Jet Propulsion Laboratory/Caltech, Pasadena, CA 91109

<sup>6</sup>University of California Irvine, Dept. Civil and Environmental Engineering, Irvine, CA 92697

## Contents of this file

1. Table S1
2. Movie S1
3. Figures S1 to S8

## 1 Introduction

In this supplementary material, we provide in Section 2 a description of how simulated heat transports were calculated along with a Table (Table S1) of net heat transports across the seven Getz cavity openings. Movie S1 shows the modeled circulation of warm water beneath the different parts of the Getz Ice shelf. In section 3, we also provide figures that highlight the geometry of the three cases considered in the ocean model simulations (Figure S1, S3), and the simulated ocean properties along the ice shelf front in those three cases (Figures S4 to S6). Figure S2 represent the differential interferograms showing the retreat of Berry Glacier. Figure S7 is a model-data comparison using the 2007 dataset of Jacobs et al. (2013). Figure S8 illustrates a section for DeVicq Glacier (similar to Figure 1).

## 2 Heat transport

The net heat transport across the seven openings of the Getz Ice Shelf cavity is computed from the model outputs according to the equation:

$$\rho_0 c_p \iint \mathbf{u}_h \left( T - T_0^{fr} \right) \cdot d\mathbf{S}, \quad (1)$$

where  $\rho_0 = 1028 \text{ kg m}^{-3}$  is a reference density for seawater,  $c_p = 4 \times 10^3 \text{ J (kg K)}^{-1}$  is the specific heat,  $\iint d\mathbf{S}$  is a surface integral for an opening of the ice shelf cavity,  $\mathbf{u}_h$  is the modeled horizontal velocity (with  $\mathbf{u}_h \cdot d\mathbf{S}$  defined positive when exiting the cavity),  $T$  is the modeled temperature of seawater,  $T_0^{fr}$  is a constant representative of the freezing temperature of seawater, and  $T - T_0^{fr}$  represents the heat available in a water parcel for basal melting. The calculation uses  $T_0^{fr} = -1.85^\circ\text{C}$  as in Jourdain et al. (2017) so that the cold Winter Water (characterized by  $T \approx -1.85^\circ\text{C}$  and occupying the upper 350 m of the Amundsen Sea (e.g., Sherrell et al., 2015)) is associated with a heat of zero and thus does not contribute to the transport of heat. Similarly, the surface integral in Equation 1 runs from the ice shelf draft (positioned at a depth of 200–300 m) to the seabed so that the shallow summer surface layer (warmed by sunlight) does not contribute to the transport of heat. Equation 1 thus represents the heat transport (in Watts) associated with modified Circumpolar Deep Water crossing the openings of the ice shelf cavity, and allows us to quantify the contribution of each opening. The heat transport is computed from the daily-averaged outputs of Cases I–III (see Methods) and then temporally-averaged over the years 2006–2008.

**Table S1.** Simulated net heat transports across the seven Getz cavity ice front openings (average of years 2006–2008). The values are negative for a net heat inflow to the cavity. Openings with significant inflows ( $< -1 \text{ TW}$ ) are bolded.  $1 \text{ TW} = 10^{12} \text{ Watts}$ .

Openings (from east to west)	Case I	Case II	Case III
	TW	TW	TW
Martin-Wright	-0.38	-0.35	-0.25
Wright-Duncan	0.52	0.86	-0.20
Duncan-Carney	0.16	0	0
Carney-Siple	0.46	0.44	0.36
Siple-Dean	<b>-2.94</b>	<b>-2.91</b>	<b>-1.59</b>
Dean-Grant	3.42	3.45	-0.12
Grant-Western edge	<b>-4.08</b>	<b>-4.06</b>	-0.39
Sum	-2.83	-2.57	-2.19

**Movie S1.** (file video\_cdw\_cases123.mp4): The video shows a numerical Eulerian tracer (“dye”) tracking warm sub-surface water within the model domain (units: parts per thousand (ppt)). The tracer is conservative (it has no sinks) and is advected/diffused by the modeled circulation. The tracer has no effect on the model’s prognostic variables and is only used to illustrate the horizontal pathways of warm water. The tracer has an initial concentration (on January 1, 2006) of zero ppt on the continental shelf. The concentration is 1000 ppt off of the shelf and at the model’s open boundaries where the sub-surface potential temperature is greater than 0.7°C. The tracer is three-dimensional and the video specifically represents the maximum concentration on the vertical at each horizontal point (i.e., the core of the tracer field). The three cases depicted in the video are described in section the Data and Methods section of the manuscript. For best results, the video should be downloaded and played on a local device.

### 3 Figures

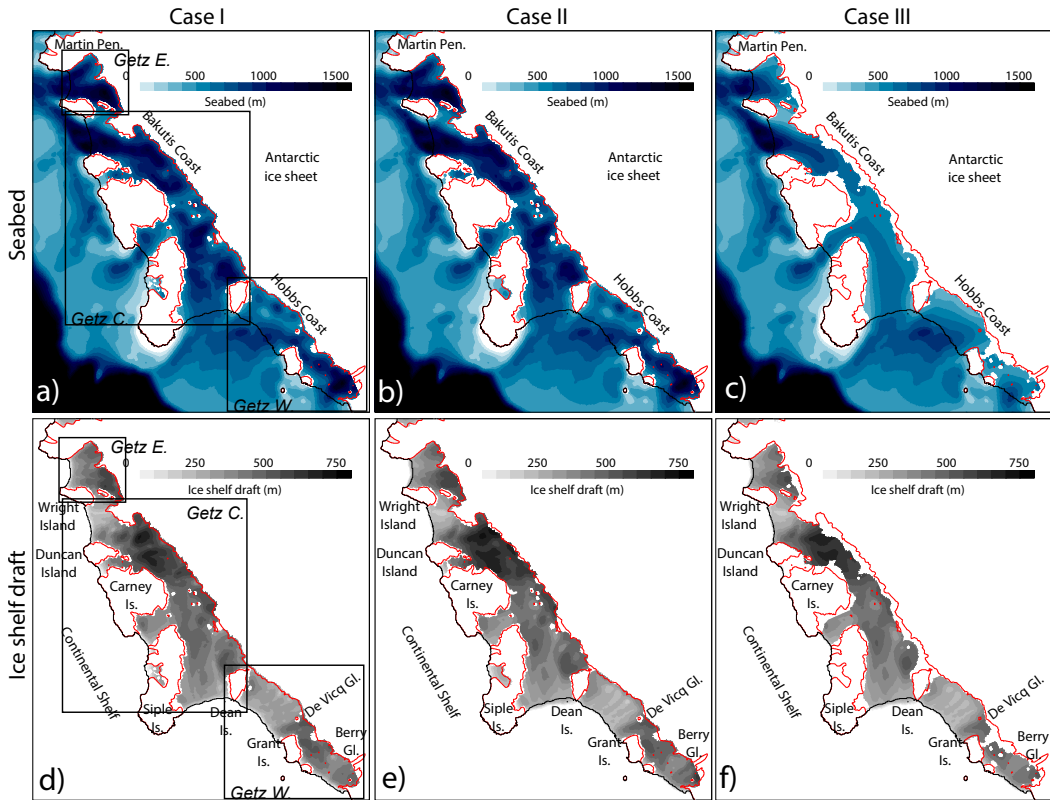


**Figure S1.** Geometry used in the simulations with the ocean model. (a,d) Case I: Seabed from the new bathymetry and ice shelf draft from BedMachine. (b,e) Case II: Seabed from the new bathymetry and ice shelf draft of RTopo-2. (c,f) Case III: Seabed and ice shelf draft of RTopo-2. Gaps in case III corresponds to water column of less than 15 m. The black and red curves represent the front and grounding line of BedMachine Antarctica (respectively).

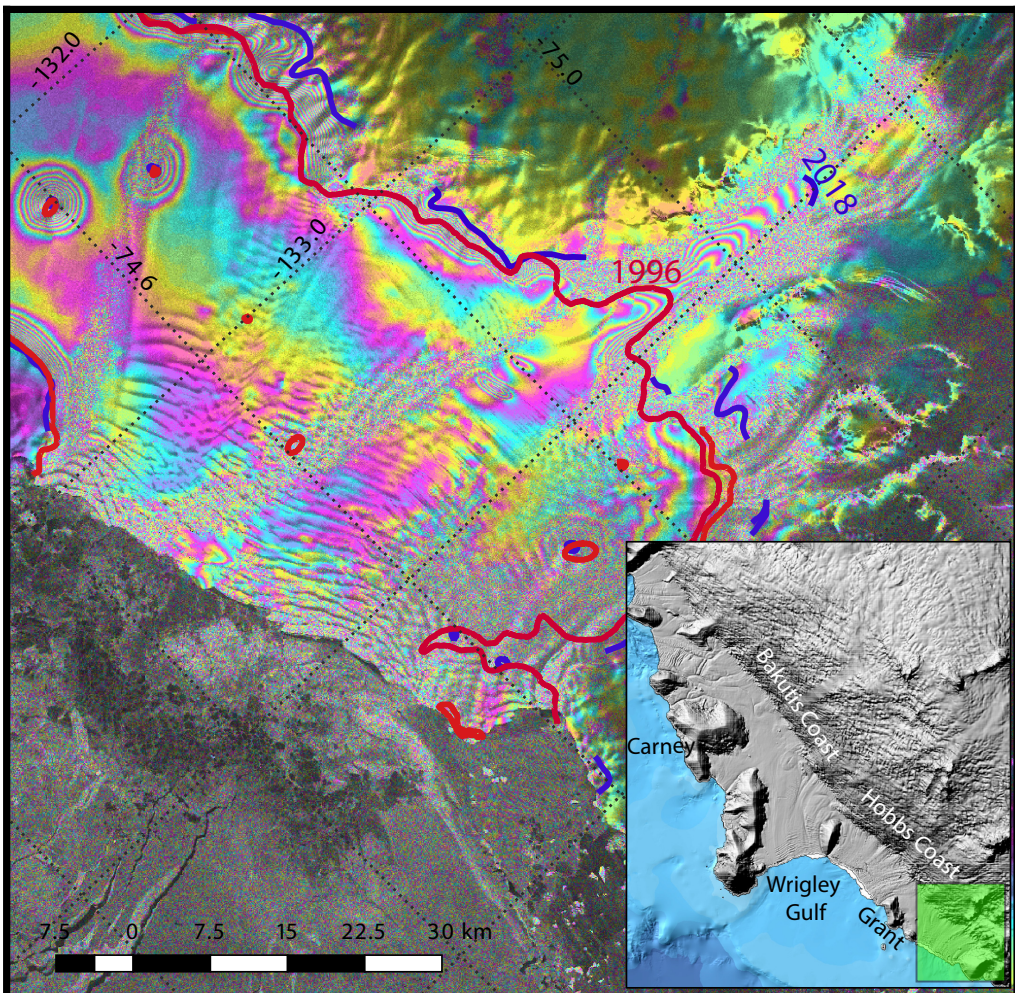


**Figure S2.** Differential interferogram over Berry Glacier obtained from Sentinel-1 satellite imagery using a repeat cycle of six days (Acquisition time of pair 1: 2018-08-14 and 2018-08-20, Acquisition time of pair 2: 2018-08-26 and 2018-09-01). The 2018 grounding line is delineated in dark blue. The 1996 grounding line is delineated in red and was obtained from pairs of ERS SAR images (Acquisition time of pair 1: 1996-02-08 and 1996-02-09, Acquisition time of pair 2: 1996-03-14 and 1996-03-15). The background is an amplitude image from Sentinel-1 scene from 2018-08-04 on grey color scale. The inset map shows the position of the interferogram.

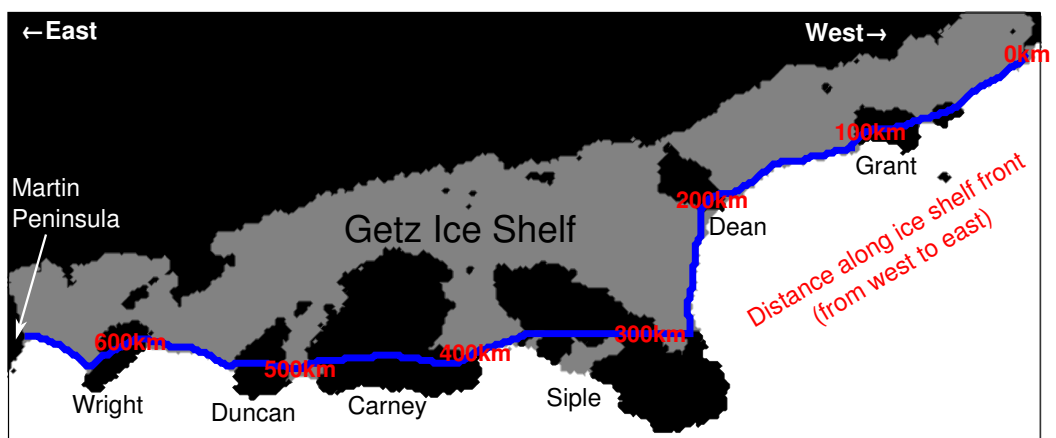


**Figure S3.** Map of the Getz Ice Shelf front with the distance along the ice shelf front labeled in kilometers (red). This distance corresponds to the horizontal axes of Figures S4-S6.

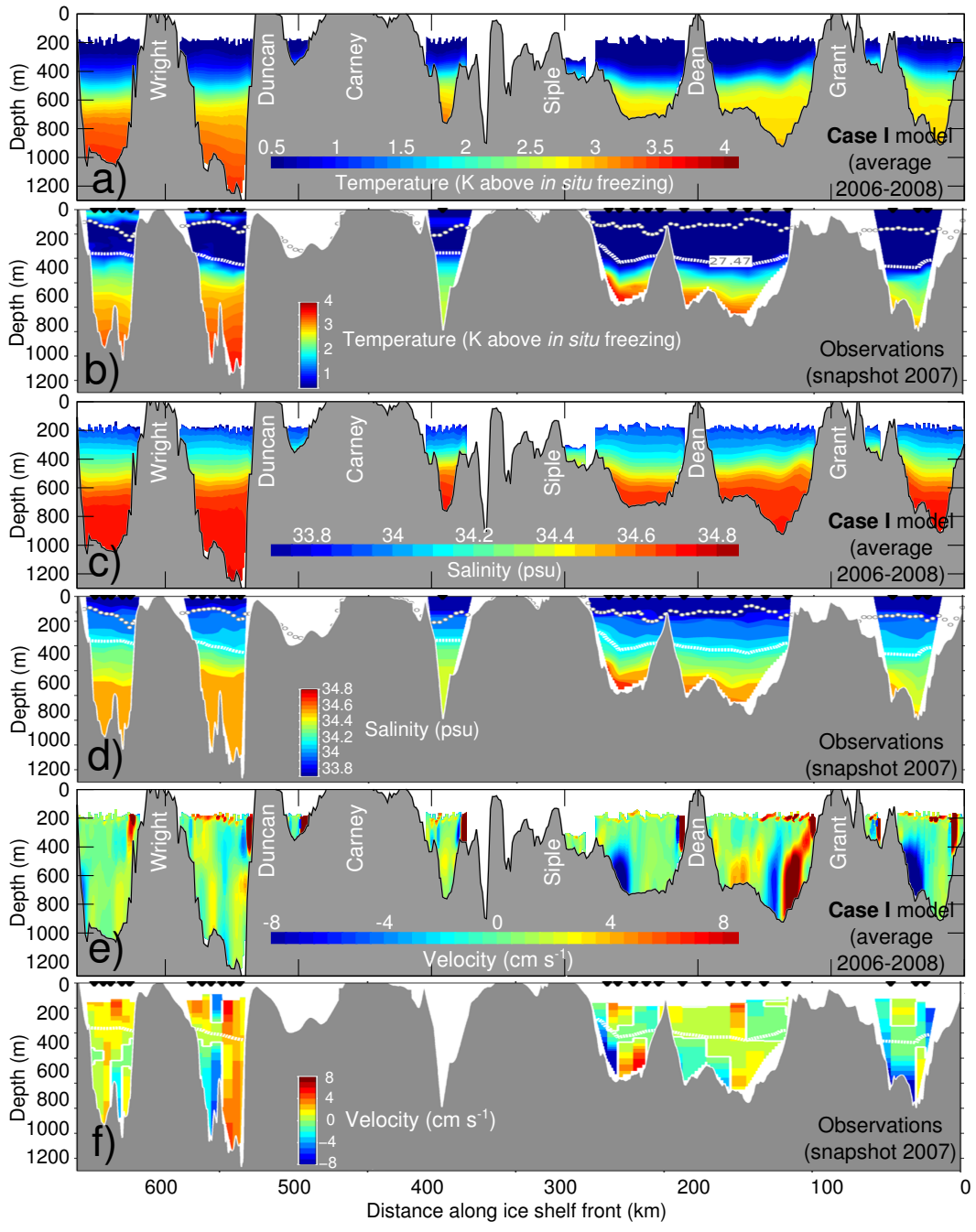


**Figure S4.** Modeled ocean properties along the ice shelf front of the Getz Ice Shelf in Case I (new bathymetry from gravity and ice shelf draft from BedMachine Antarctica). Results show an average of years 2006–2008. (a) Temperature above the *in situ* freezing temperature, (c) salinity, (e) velocity (positive out of the cavity). (b,d,f) Same as a,c,e but from observations collected in 2007 (figures modified from Jacobs et al. (2013)). The scales in (a) and (b) are in Kelvin rather than °C to emphasize that temperature is referenced to the *in situ* seawater freezing point. White dashed lines show the surface-referenced 27.47 potential density anomaly. White dotted line represent the ice shelf front.

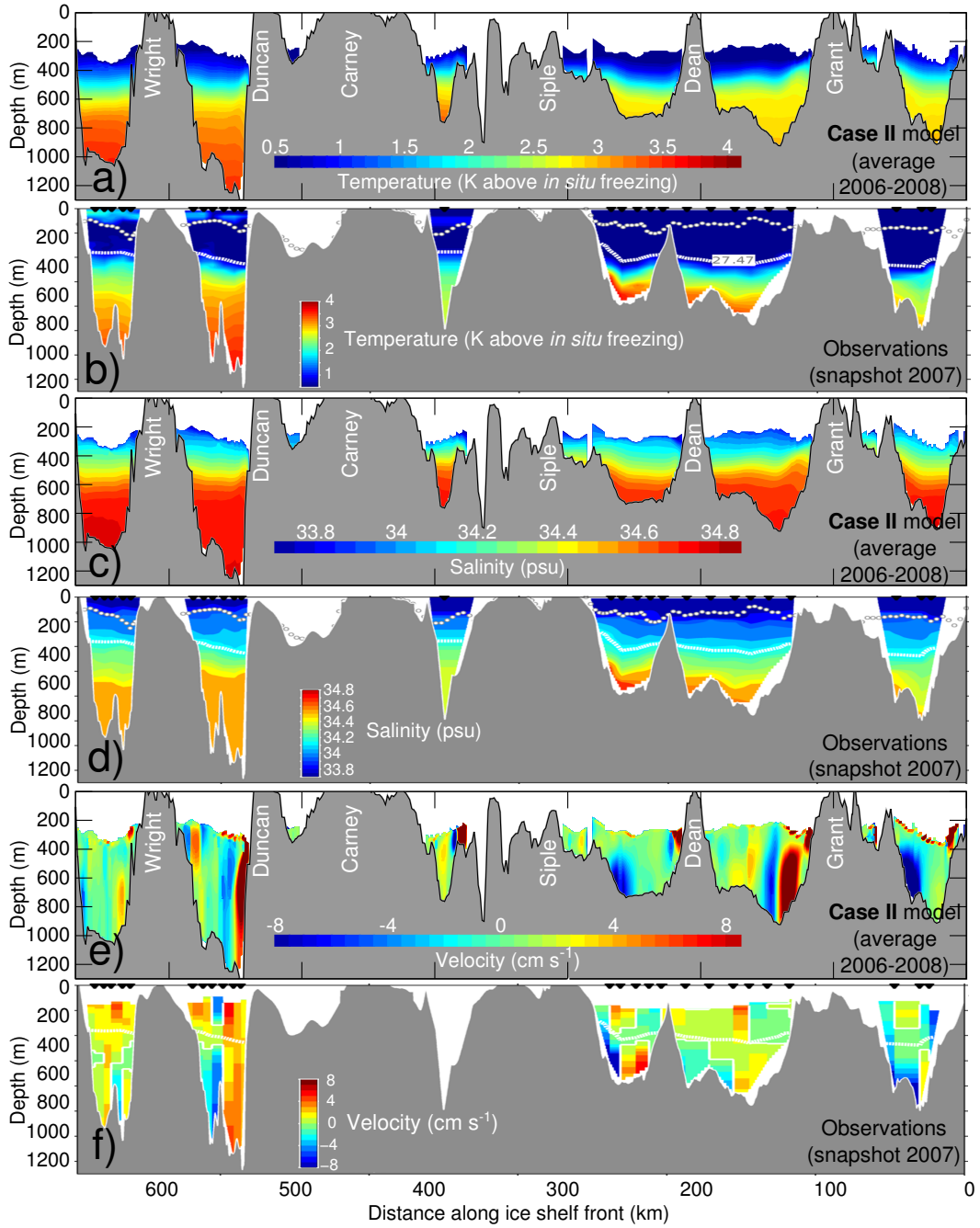


**Figure S5.** Same as Figure S4 but for Case II (new bathymetry from gravity and ice shelf draft from RTopo-2). (a,b) Temperature above the *in situ* freezing temperature, (c,d) salinity, (e,f) velocity (positive out of the cavity).

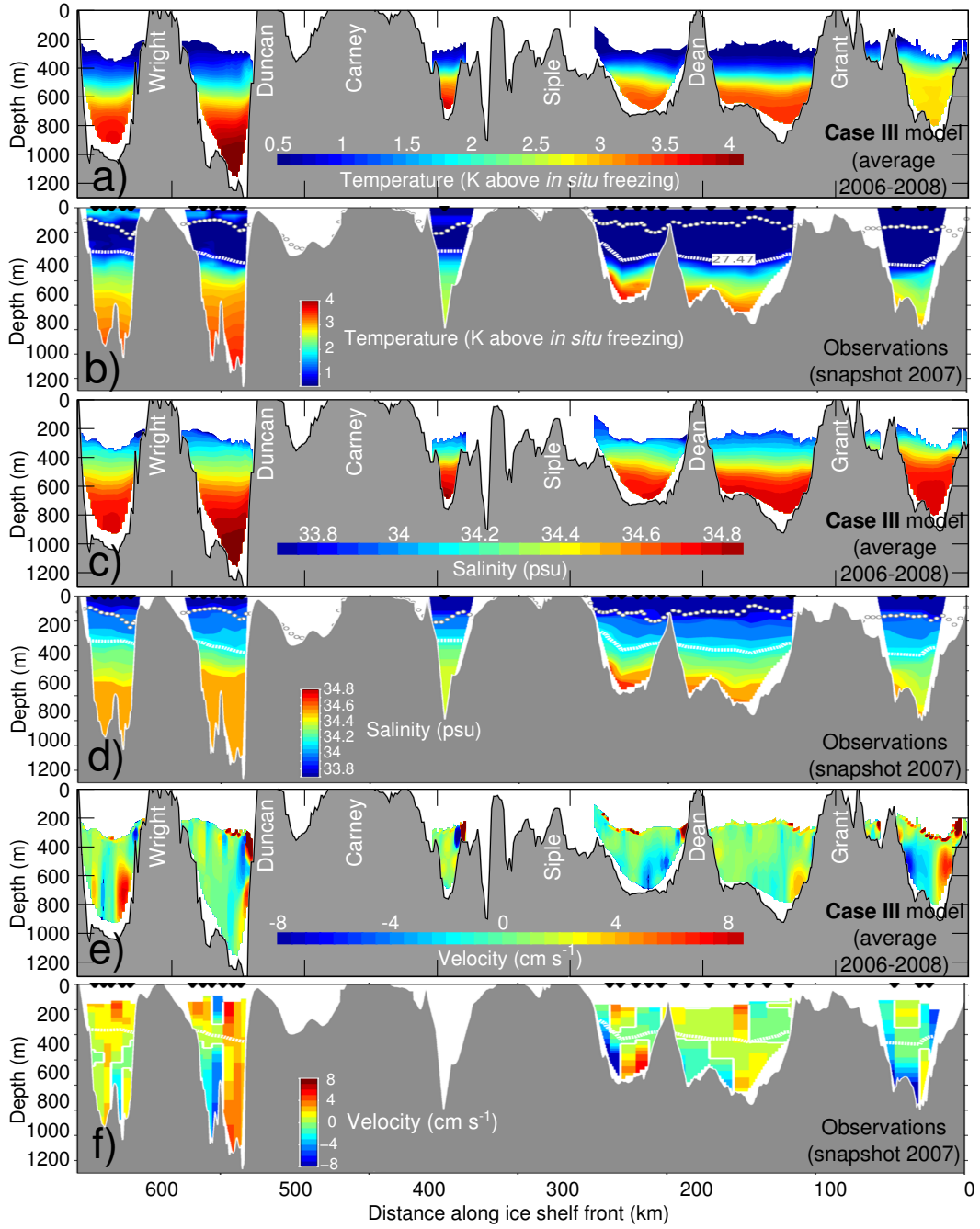


**Figure S6.** Same as Figure S4 but for Case III (bathymetry and ice shelf draft from RTopo-2).

(a,b) Temperature above the *in situ* freezing temperature, (c,d) salinity, (e,f) velocity (positive out of the cavity). In a,c,e, the white gap near the sea floor is due to the fact that the model bathymetry of Case III is shallower than in Cases I-II.

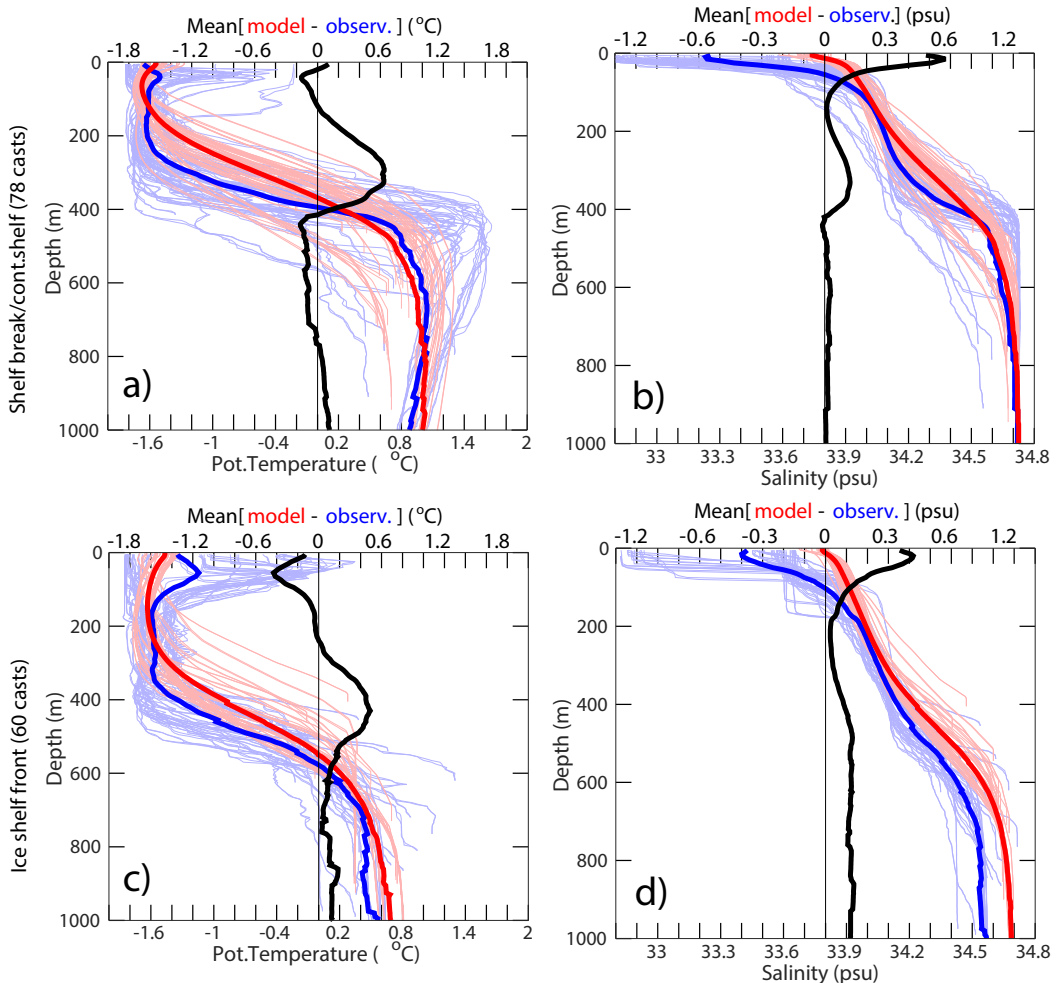


**Figure S7.** Model-data comparison for temperature and salinity using the 2007 dataset of Jacobs et al. (2013). The model results are from Case I and are averaged over years 2006–2008. The cruise data were obtained from World Ocean Database ([https://www.nodc.noaa.gov/OC5/WOD/pr\\_wod.html](https://www.nodc.noaa.gov/OC5/WOD/pr_wod.html)) and cover the period Feb., 18, 2007 to March 18, 2007 (austral summer/spring). Casts collected west of Dotson Ice Shelf (i.e., west of  $114^{\circ}\text{W}$ ) were selected and divided into two groups: casts from the shelf break and continental shelf (north of  $73.8^{\circ}\text{S}$ ; 78 casts), and casts near the Getz Ice Shelf front (i.e., south of  $73.8^{\circ}\text{S}$ , 60 casts; note that these numbers include both upcasts and downcasts). The modeled temperature and salinity were extracted from the grid cell positioned closest to each cast. (a) Observed (light blue) and modeled (light red) temperature casts at the shelf break and on the continental shelf. The average of the individual casts is represented with a thick dark blue line (observations) and a thick dark red line (model). The black line is the average model bias. (b) Same as a, but for salinity. (c) Same as a, but for the casts collected near the Getz Ice Shelf front. (d) Same as c, but for salinity.

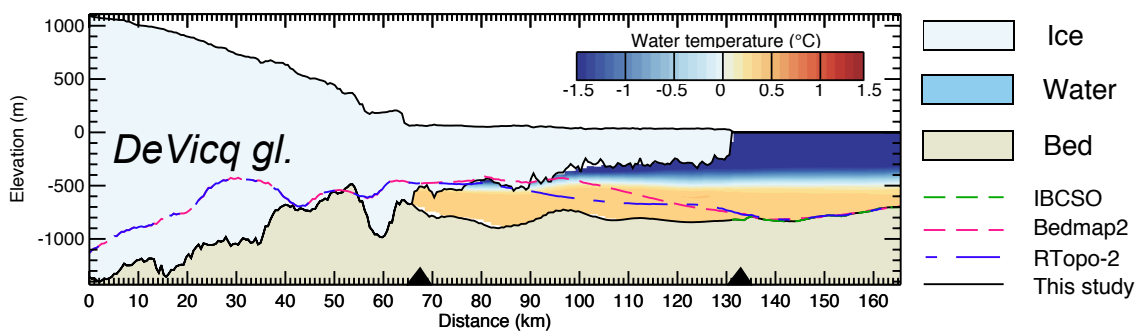


**Figure S 8.** Surface elevation along C-C' (cf figure 1 for profile position) with bed elevation from this study (black), BEDMAP-2 (red dotted line), and multibeam echo sounding (dashed green) of DeVicq Glacier. Ice is light blue, seabed is light brown, and the ocean is shaded with the water temperature from the 3D ocean model (average of years 2006-2008). The inversion boundaries are shown as black triangles.

## References

- Jacobs, S., Giulivi, C., Dutrieux, P., Rignot, E., Nitsche, F., & Mouginot, J. (2013). Getz ice shelf melting response to changes in ocean forcing. *J. Geophys. Res.*, 118, 1-17. doi: <https://doi.org/10.1002/jgrc.20298>
- Jourdain, N. C., Mathiot, P., Merino, N., Durand, G., Sommer, J. L., Spence, P., ... Madec, G. (2017). Ocean circulation and sea-ice thinning induced by melting ice shelves in the amundsen sea. *J. Geophys. Res. Oceans*, 122, 2550-2573. doi: <https://doi.org/10.1002/2016JC012509>
- Sherrell, R. M., Lagerstrom, M. E., Forsch, K. O., Stammerjohn, S. E., & Yager, P. L. (2015). Dynamics of dissolved iron and other bioactive trace metals (Mn, Ni, Cu, Zn) in the Amundsen Sea Polynya, Antarctica. *Elem. Sci. Anthropocene*, 3(71). doi: <https://doi.org/10.12952/journal.elementa.000071>